ORIGINAL PAPER

Palladium(II) complexes assembled on solid materials: as catalysts for the –NO$_2$ (nitro) to –NH$_2$ (amine) reactions

Serkan Dayan[1] · Nilgün Kayacı[2] · Namık Özdemir[3] · Osman Dayan[4] · Nilgun Kalaycioglu Ozpozan[2]

Abstract

Herein, a new series of [PdCl$_2$(L)$_2$] complexes where ligands are monodentate amine ligands bearing sulfonamide groups were synthesized, characterized using various techniques such as NMR, FT-IR, UV–Vis, and sc-XRD and investigated for their catalytic performance for the reduction of nitroarenes (2-nitroaniline, 4-nitroaniline, and nitrobenzene) in the presence of NaBH$_4$ in water under heterogeneous conditions. Because the results show that the synthesized complexes are very efficient catalysts, materials using the selected palladium(II) complex supported by multiwall carbon nanotubes, silicon dioxide, and iron(II,III) oxide (Fe$_3$O$_4$) were fabricated by a simple-impregnation methodology, characterized by FT-IR, BET, TEM, and XRD techniques and investigated for their catalytic performance for the same reaction. Thus, a series of supported catalysts was designed with the aim of both enhancing catalytic activity and reducing noble-metal contents. Our findings serve to develop simple catalytic systems and this system can be easily used for catalytic reduction reactions which are the cornerstone of the production of important chemicals.

Graphic abstract
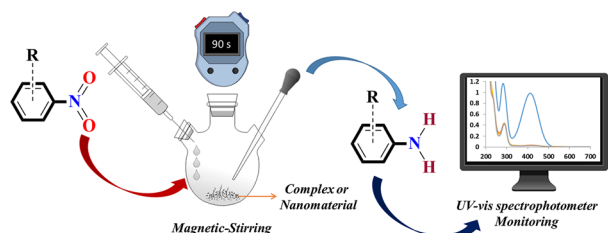
Keywords Palladium(ii) complexes · Supported catalysts · Nitrobenzene · Hydrogenation

---

✉ Serkan Dayan
serkandayan@erciyes.edu.tr

1 Drug Application and Research Center, Erciyes University, 38039 Kayseri, Turkey

2 Department of Chemistry, Faculty of Science, Erciyes University, 38039 Kayseri, Turkey

3 Department of Mathematics and Science Education, Faculty of Education, Ondokuz Mayıs University, 55139 Samsun, Turkey

4 Department of Chemistry, Faculty of Science, Çanakkale Onsekiz Mart University, 17020 Çanakkale, Turkey

Introduction

Nitro compounds are widely regarded as contaminants found in industrial waste and they pose a serious problem for both living organisms and the ecosystem. Also, amine compounds formed by the hydrogenation of nitro compounds are used in many areas as qualified chemicals; for example, as chelating agents in pharmaceuticals, polymers, pesticides, explosives, fibers, dyes, and cosmetics, etc. [1–7]. The most suitable method to produce aromatic amines which belong to the group of compounds that are more useful than nitrobenzene derivatives is an efficient, environmentally friendly, catalytic system operating in mild conditions. In this case, many processes have been developed, including adsorption/

desorption, photoactive catalysts, electrochemical treatment, the e-Fenton method, electrocoagulation, hydrogenation, etc. [8–13]. The development of a catalytic system undergoes several reaction optimizations steps. Among these, substrate-related screening tests, as well as the development of suitable catalysts and, studies about increasing the activity of existing catalysts can be quite valuable. In general, the catalytic hydrogenation of nitrobenzene derivatives is made possible by catalysts containing many metals. For example, palladium, platinum, gold, and silver are the most common ones, and their catalytic performances are excellent. However, the high price of noble metals used during the catalytic process is the main disadvantage of these conventional noble-metal catalysts and limit their large-scale applications. The catalysts including other metals may also lose catalytic performance. Therefore, the idea of adding materials that can add a synergistic effect to catalysts consisting of noble metals has also been investigated by researchers. Of course, many parameters come to the fore in these catalytic systems; for example, solvent, hydrogen source, amount of substrate, amount of catalyst, etc. [14–17].

Also, avoiding the use of organic solvents and the improvement of suitable processes for hydrogenation of nitrobenzenes in aqueous media under mild conditions are still necessary. Likewise, some quite remarkable studies have been carried out with compounds bearing palladium for the hydrogenation of nitro-compounds [18–27].

Complexes or materials containing palladium are also widely used during the application of reduction processes [28], C–C or C–N bond formation reactions [29, 30], oxidation works [31, 32], hydrogenation studies [33], anti-cancer drugs [34, 35], as biosensors [36], in solar cells [37], etc. Especially, palladium complexes or materials have been the focus of intense research in catalyst chemistry as a homogeneous/heterogeneous catalyst [38–40]. From most of the research about palladium complexes in the literature, it is seen that at least bidentate ligands were used, because electronic and steric parameters are one of the most important cases in catalysis chemistry. The research about Pd(II) complexes with monodentate ligands is rare. On the other hand, the preparation conditions for Pd(II) complexes bearing N-donor ligands generally does not require a specific atmosphere such as argon or nitrogen gas. Recently, palladium-based catalysts, in particular, those supported by carbon [41], zeolite [42], silica [43], alumina [44], and polymer [45], have been fabricated by different methods (such as deposition–precipitation, impregnation and co-precipitation, immobilization, etc.) and used as catalysts in many organic transformations (C–C bond formation, hydrogenation, oxidation, etc.).

The studies of combining molecular and material structures with immobilization methods have been frequently seen in recent years [26, 37, 46–48]. In this way, the materials containing different characteristic properties are combined with a simple method. These new materials can also show synergistic effects in different application areas.

Because of all these reasons, there is increasing attention in the literature about the preparation of simple, novel, effective, and reusable catalysts for catalytic reduction of nitro compounds in aqueous media. For these purposes, herein, we report a new series of synthesized Pd(II) complexes C_1–C_6 bearing monodentate N-(2-aminophenyl)benzenesulfonamides ligands which can easily interact with supporting materials via secondary chemical bonding and tested as catalysts for the reduction of nitrobenzenes. Herein the sulfonamides ligands are easily synthesizable compounds, and the sulfonamide compounds support the immobilization methodology with the functional groups. In addition, sulfonamide derivative ligands and their complexes are often used in catalytic reactions [48–50].

Then, to reduce noble-metal (Pd) content, the MWCNT, SiO_2, and Fe_3O_4-supported C_4 materials M_1–M_3 were also prepared and screened for their efficiency as catalysts in the reduction of nitroarenes. The catalytic results for the supported materials clearly show that although the palladium content is reduced, the catalytic efficiencies are higher than for the complexes.

Results and discussion

The details of analytical methods

The synthesis of monoamine aromatic sulfonamide ligands L_1–L_6 was performed in a simple one-step reaction, starting from commercially available arylsulfonyl chlorides and 1,2-diaminobenzene. Their amine-coordinated Pd(II) complexes C_1–C_6 were isolated as yellow solids with high yields and were stable in the solid-state and solution. The structures of Pd(II) complexes C_1–C_6 were elucidated by FT-IR, NMR, and UV–Vis spectrophotometer.

In ^1H NMR spectra recorded from a Bruker 400 NMR spectrometer at 297 K, the methoxy and 2,4,6-trimethyl protons for C_2 and C_4 were assigned at 3.81 ppm as singlet for –OCH_3 group, at 2.24 ppm as singlet for -p-CH_3 and 2.38 ppm as singlet for o-CH_3 for 2,4,6-trimethyl protons, respectively. Also, the aromatic ring protons as multiplet peaks were located at 6.72–7.99 ppm for C_1, 6.49–7.60 ppm for C_2, 6.46–8.37 ppm for C_3, 6.45–7.09 ppm for C_4, 6.75–8.02 ppm for C_5, and 6.75–7.95 ppm for C_6. In the ^{13}C NMR spectra for the N-coordinate Pd(II) complexes C_1–C_6, the peaks belonging in (c) position to the -p-OCH_3, -p-CH_3 carbons were located at 55.6 ppm and 22.6 ppm, respectively. Additionally, the carbons belonging to aromatic rings were obtained at 117.1–147.2 ppm for C_1, 113.8–162.3 ppm for C_2, 124.2–149.7 ppm for C_3, 116.7–147.3 ppm for C_4,

115.7–147.0 ppm for **C$_5$**, and 121.0–146.9 ppm for **C$_6$**. All NMR chemical shifts and integrations of signals were consistent with the proposed structures (Fig. S$_{1–8}$). FT-IR was measured with a Perkin-Elmer Spectrum 400 FTIR system. For the palladium(II) complexes **C$_1$**–**C$_6$**, the –N–H stretching frequency peaks belonging to the sulfonamide groups appeared at 3098 cm^{-1}, 3131 cm^{-1}, 3147 cm^{-1}, 3153 cm^{-1}, 3109 cm^{-1}, and 3152 cm^{-1} and -NH$_2$ stretching frequency peaks were observed at 3252–3148 cm^{-1}, 3279–3165 cm^{-1}, 3300–3216 cm^{-1}, 3269–3185 cm^{-1}, 3221–3153 cm^{-1}, and 3247–3185 cm^{-1}, respectively.

The UV–Vis spectra of Pd(II) complexes **C$_1$**–**C$_6$** in dimethyl sulfoxide (DMSO) (1×10^{-4} mol dm^{-3}) solvent were recorded within the 260–560 nm range, and a representative spectrum is shown in Fig. S9. In the spectra of the complexes, there are two main transition bands excluding **C$_6$** complex. The first bands (280–301 nm) are attributed to the $\pi \rightarrow \pi^*$ transition and the second bands in the range of 326–335 nm are attributed to the $n \rightarrow \pi^*$ transition of the Pd(II) complexes.

Description of the crystal structure of C$_1$

X-ray data were collected with an STOE IPDS II diffractometer at room temperature using graphite-monochromated Mo Kα radiation by applying the ω-scan method. Data collection and cell refinement were carried out using X-AREA, while data reduction was applied using X-RED32 (X-AREA Version 1.18 and X-RED32 Version 1.04, Stoe & Cie, Darmstadt, Germany, 2002). The structure was solved by direct methods using SHELXS-2013 and refined with full-matrix least-squares calculations on F^2 using SHELXL-2014 [51, 52] implemented in WinGX [53] program suit. H atoms bonded to C atoms were assigned C–H distances of 0.93 Å, with $U_{iso}(H) = 1.2U_{eq}(C)$. The nitrogen-bound hydrogens were in a difference Fourier map and refined freely. Crystal data, data collection and structure refinement details are summarized in Table 1, while relevant geometric parameters are collected in Table 2. PLATON was used for the structure analysis. Molecular graphics were generated using ORTEP-3 [53].

The molecular structure of complex **C$_1$** was confirmed using the X-ray crystallography. The compound crystallizes in the triclinic space group $P\bar{1}$ with a single molecule in the unit cell and is shown in Fig. 1.

The asymmetric unit of the compound contains one-half of the molecule, because the palladium atom occupies a special position in the crystallographic center of inversion. The Pd(II) cation is coordinated to two chlorido ligands and the nitrogen atoms of two *N*-(2-aminophenyl)-benzenesulfonamide ligands, in an almost perfect square-planar geometry. The molecule adopts the *trans* disposition, which is commonly observed for bis(amino)-dihalopalladium(II)

complexes [54, 55]. The N−Pd−Cl *cis* angles [89.66(4)–90.34(4)°] are very close to the optimal angle of 90°, while the Cl−Pd−Cl and N−Pd−N *trans* angles are exactly equal to 180°. The bond distances for Pd−N [2.0623(14) Å] and Pd−Cl [2.2850(4) Å] are comparable with those published in the literature for related complexes of general formula PdCl$_2$L$_2$, where L denotes the amino-ligands [54–61]. The square plane makes dihedral angles of 86.22(5)° and 65.53(6)° with the planes of the C1–C6 and C7–C12 benzene rings, while the dihedral angle between the two benzene rings is 64.30(7)°. In the benzenesulfonamide ligand, the N1–C7 and N2–C12 bond distances of 1.414(2) and 1.442(2) Å agree well with the single bond value, and the S1–O1 and S1–O2 distances of 1.4351(19) and 1.4213(19) Å are consistent with S=O double bonding. Atom S1 has a distorted tetrahedral configuration which is evident from the angles changing from 105.21(10)° to 120.49(13)°.

In the molecular structure of the complex, there are two intramolecular interactions of N−H⋯Cl type (Fig. 1), forming seven-membered rings with graph-set descriptor $S(7)$ [62]. The 2D supramolecular structure of the complex can readily be analyzed in terms of two one-dimensional substructures. In the first substructure, amino atom N2 in the molecule at (x, y, z) acts as a hydrogen-bond donor, via atom H2B, to sulfonyl atom O1 in the molecule at ($x − 1$, y, z), thereby forming an $R_2^2(18)$ ring. The propagation of this hydrogen-bonding motif generates a chain of rings running parallel to the [100] direction (Fig. 2a). In the second substructure, benzene carbon atom C10 in the molecule at (x, y, z) acts as a hydrogen-bond donor to chlorido ligand Cl1 in the molecule at ($− x − 1$, $− y + 1$, $− z + 1$), so forming an $R_2^2(14)$ ring. Propagation of this hydrogen-bonding motif generates another chain of rings running parallel to the $\left[1\ \bar{1}\ 0\right]$ direction (Fig. 2b). Full details of the hydrogen-bonding geometry are given in Table 3.

Materials' characterization

The infrared spectrum of multiwall carbon nanotubes (MWCNTs)–, SiO$_2$–, and Fe$_3$O$_4$– supported **M$_1$**–**M$_3$** materials and **C$_4$** are shown in Fig. 3. For **M$_1$** (Fig. 3a), the carbonyl (C=O), the C=C stretching, and the –OH bending absorption bands were associated with ≈ 1800 and 1100–1300 cm^{-1}, ≈ 1500–1600 cm^{-1} and ≈ 3500–3800 cm^{-1} and were compatible with bare MWCNTs-COOH, respectively. For **M$_2$** (Fig. 3b), the bare SiO$_2$ has two major peaks at 794 and 1047 cm^{-1} which are attributed to Si–O bending and Si–O–Si asymmetric stretching, respectively and the related major peaks were also observed in the FT-IR spectra of **M$_2$** material. For **M$_3$**, the absorption band at 529 cm^{-1} belongs to the Fe–O vibration (magnetic phase). Hereby, the formation

Table 1 Crystal data and structure refinement parameters for C_1

CCDC depository	1,483,076
Color/shape	Dark orange/prism
Chemical formula	$[PdCl_2(C_{12}H_{12}N_2O_2S)_2]$
Formula weight	673.89
Temperature/K	296
Wavelength/Å	0.71073 Mo Kα
Crystal system	Triclinic
Space group	$P\bar{1}$ (No. 2)
Unit cell parameters	
a, b, c/Å	7.2484(4), 8.2098(5), 12.3917(8)
α, β, γ/°	73.068(5), 82.842(5), 72.361(5)
Volume/Å^3	671.74(7)
Z	1
D_{calc}/g cm^{-3}	1.666
μ/mm^{-1}	1.084
Absorption correction	Integration
T_{min}, T_{max}	0.5652, 0.7390
F_{000}	340
Crystal size/mm^3	0.56×0.49×0.33
Diffractometer/measurement method	STOE IPDS II/ω scan
Index ranges	$-9 \leq h \leq 9, -11 \leq k \leq 11, -16 \leq l \leq 16$
θ range for data collection/°	$2.702 \leq \theta \leq 28.639$
Reflections collected	10,635
Independent/observed reflections	3431/3282
R_{int}	0.102
Refinement method	Full-matrix least-squares on F^2
Data/restraints/parameters	3431/0/181
Goodness-of-fit on F^2	1.061
Final R indices [$I > 2\sigma(I)$]	$R_1 = 0.0228$, $wR_2 = 0.0597$
R indices (all data)	$R_1 = 0.0307$, $wR_2 = 0.0604$
$\Delta\rho_{max}, \Delta\rho_{min}$ /e Å^{-3}	0.473, $-$0.311

Table 2 Selected geometric parameters for C_1

| Bond lengths/Å			
Pd1–Cl1	2.2850(4)	S1–N1	1.6286(17)
Pd1–N2	2.0623(14)	S1–C6	1.7592(19)
S1–O1	1.4351(19)	N1–C7	1.414(2)
S1–O2	1.4213(19)	N2–C12	1.442(2)
Bond angles/°			
Cl1–Pd1–Cl1^i	180.0	O1–S1–N1	105.21(10)
N2–Pd1–N2^i	180.0	O2–S1–C6	107.96(11)
N2–Pd1–Cl1	90.34(4)	O1–S1–C6	107.35(10)
N2–Pd1–Cl1^i	89.66(4)	N1–S1–C6	107.16(8)
O2–S1–O1	120.49(13)	C7–N1–S1	122.29(13)
O2–S1–N1	108.01(11)		

Symmetry code: ^{i} $-x, -y, -z+1$

of peaks belonging to the C_4 complex does not appear in the initial curve of the support materials (MWCNT, SiO$_2$, Fe$_3$O$_4$).

The bare MWCNT, SiO$_2$, and Fe$_3$O$_4$ support appear as (a), (b), and (c) in Fig. 3, respectively, and the formation of peaks belonging to Pd(II) complex C_4 is seen in Fig. 3. In brief, it was found that the Pd(II) complex C_4 is supported by MWCNT, SiO$_2$, and Fe$_3$O$_4$ after the use of the impregnation method.

Transmission electron microscopy (TEM) images were taken by the JEOL TEM-1400-EDX model device. Figure 4a–c and S10 show a representative TEM image of the prepared M_1–M_3 materials, respectively. When investigating the TEM image, it can be concluded that the characteristic shapes belonging to MWCNT, SiO$_2$, and Fe$_3$O$_4$ were preserved after impregnation. Also, the EDX images are given in Fig. S11 as supporting information.

The Barrett–Joyner–Halenda (BJH) pore volume (cm^3 g^{-1}), Brunauer–Emmett–Teller (BET) surface area
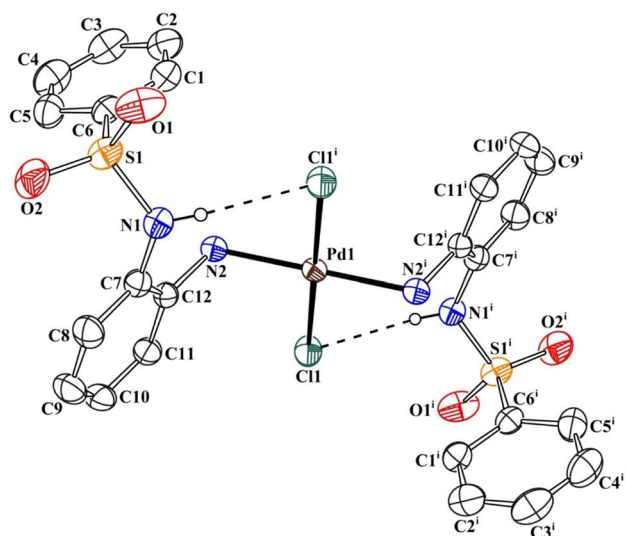
Fig. 1 Molecule of **C$_1$** showing the atom-labeling scheme. Displacement ellipsoids are drawn at the 30% probability level. Hydrogen bonds are shown as dashed lines. For the sake of clarity, only hydrogen atoms involved in hydrogen bonding have been included

(m^2 g^{-1}), and BJH pore width (Å) were calculated by the N$_2$ adsorption–desorption (BET) isotherms for **M$_1$**–**M$_3$** using a Micromeritics Gemini VII Surface Area and Porosity system. The results indicate that the BET isotherms of **M$_1$**–**M$_3$** materials were identified as typical type IV isotherms according to IUPAC (Fig. 5). The BET surface areas (S_{BET}) of **M$_1$**–**M$_3$** were found as 125.59 m^2 g^{-1}, 2.989 m^2 g^{-1}, and 54.815 m^2 g^{-1}, respectively. The S_{BET} surface area of **M$_1$** is high compared to **M$_2$** and **M$_3$** (Table 4). Table 4 shows the corresponding BJH pore widths of 531.375 Å, 484.197 Å, and 152.692 Å, respectively. Also, all the N$_2$ adsorption–desorption (BET) isotherms data is give in the supporting information as Table S1. As expected, the surface area of the carbon nanotube structure (MWCNTs) was observed higher than other solid support materials. It is well known that the surface area is an important parameter in catalyst systems and has catalytic efficiency increasing effect. Likewise, the surface area of the Fe$_3$O$_4$ solid support is well and it is predicted that it contributes positively to the catalytic yield.

X-ray powder diffraction (XRD) analyses were measured with a Bruker AXS D8 Advance Model diffractometer which
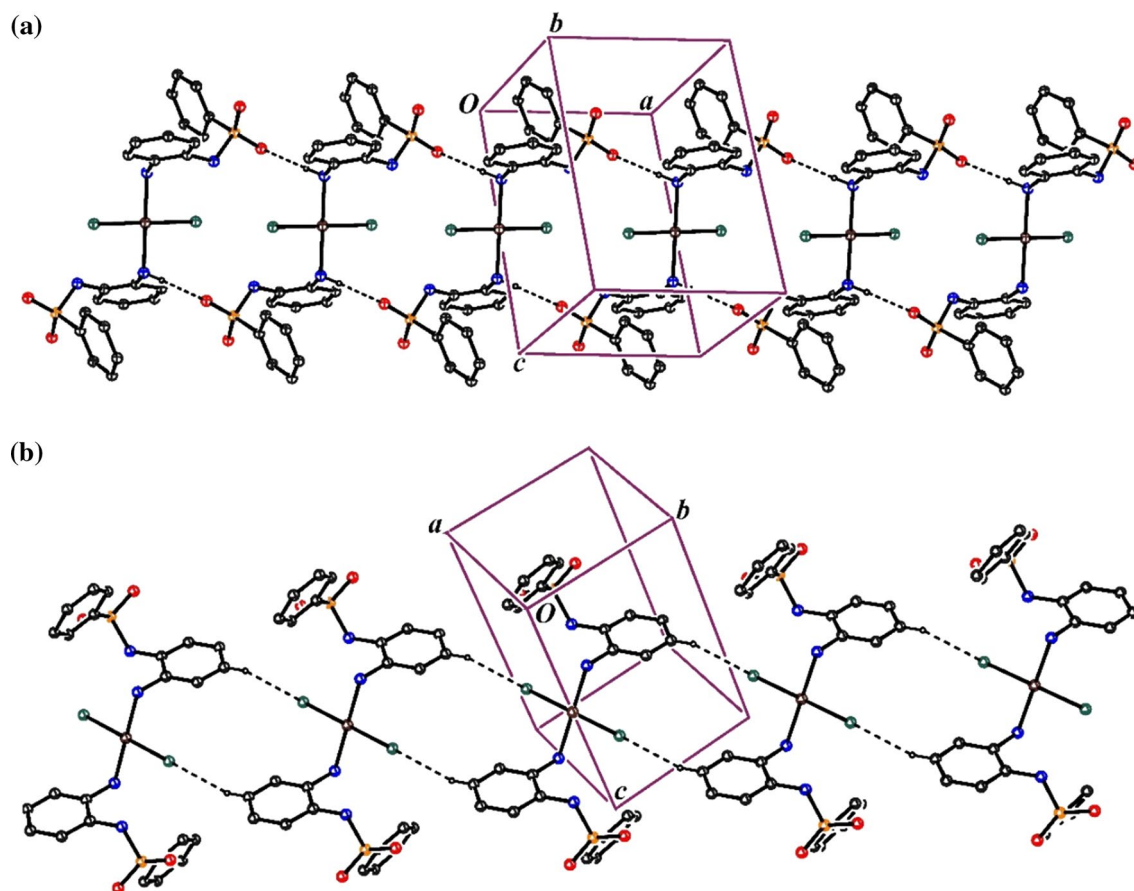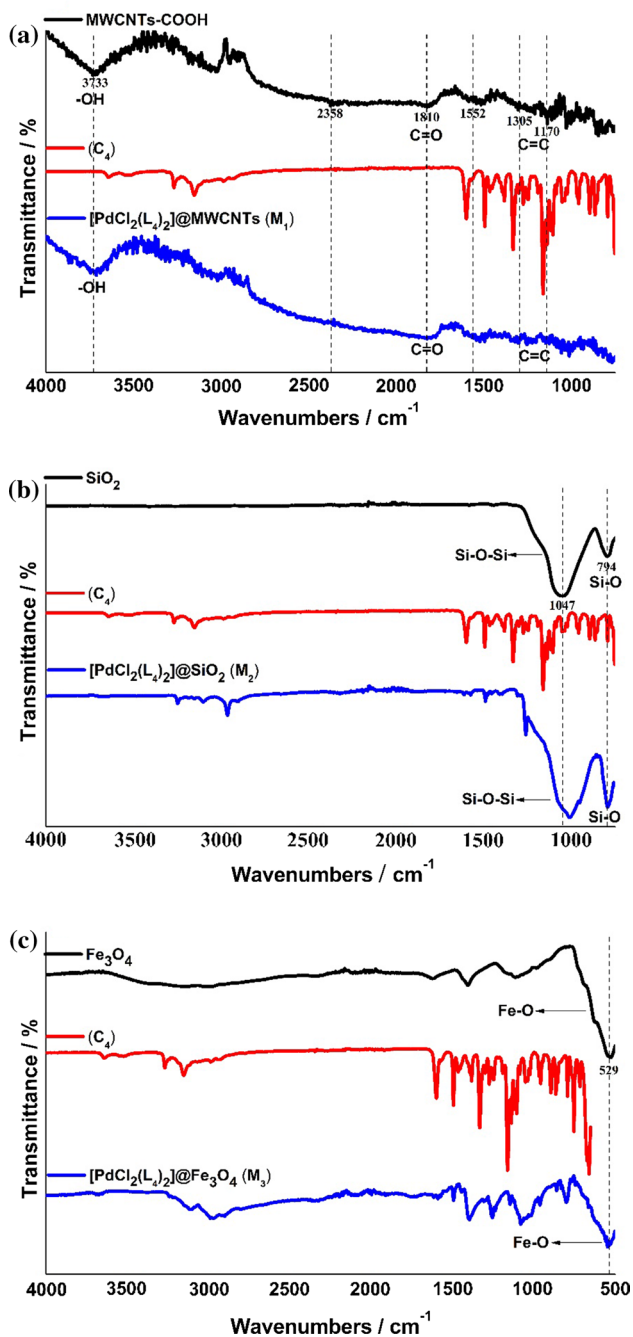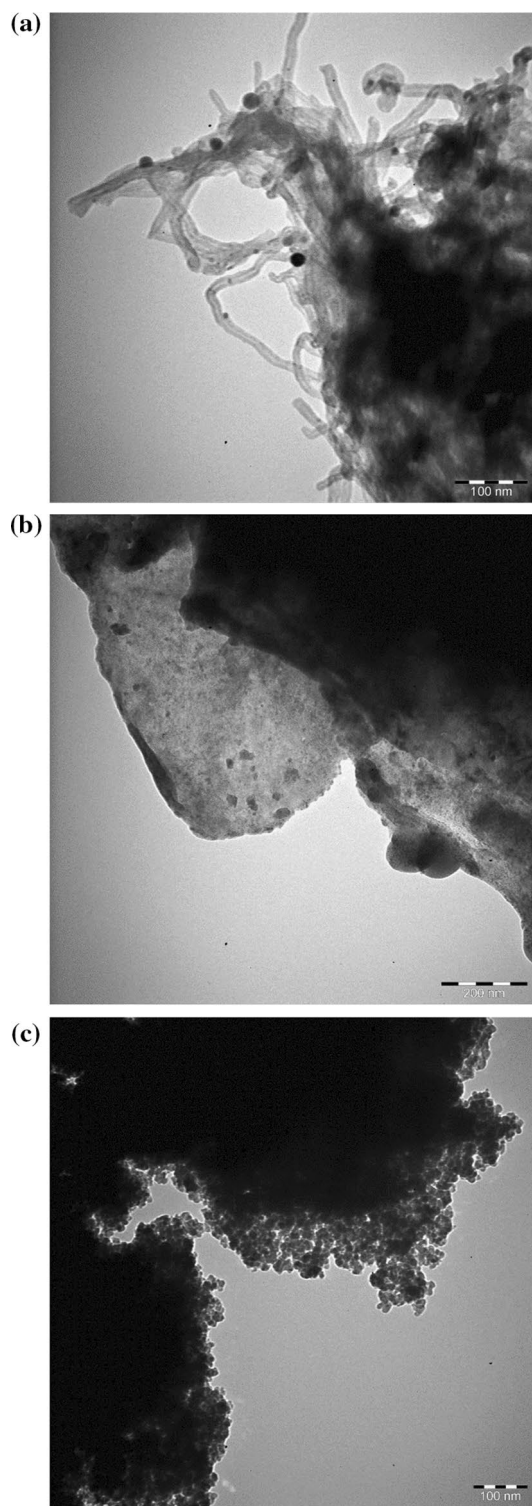

Fig. 2 **a** Part of the crystal structure of **C$_1$** showing the formation of a chain of $R_2^2(18)$ rings along [100]. **b** Part of the crystal structure of **C$_1$**, showing the formation of a chain of $R_2^2(14)$ rings along $\left[1\,1\,0\right]$.

For the sake of clarity, H atoms not involved in the motif shown have been omitted

Table 3 Hydrogen-bonding geometry for C_1

D–H···A	D–H/Å	H···A/Å	D···A/Å	D–H···A/°
N1–H1A···Cl1[i]	0.80(2)	2.49(2)	3.2490(18)	159(2)
N2–H2B···O1[ii]	0.83(2)	2.14(2)	2.966(2)	175(2)
C10–H10···Cl1[iii]	0.93	2.73	3.626(2)	161

Symmetry codes: [i] $-x, -y, -z+1$; [ii] $x-1, y, z$; [iii] $-x-1, -y+1, -z+1$

Fig. 4 Representative TEM images of M_1 (**a**), M_2 (**b**), and M_3 (**c**)

Fig. 3 FT-IR spectra prepared materials

was run at 20–60 kV and 6–80 mA, $2\Theta = 10°–90°$, and a step of 0.002° using CuKα X-ray. Powder XRD studies were performed to analyze the formation of patterns. The XRD spectra demonstrated that all the Pd(II)-impregnated MWCNT,
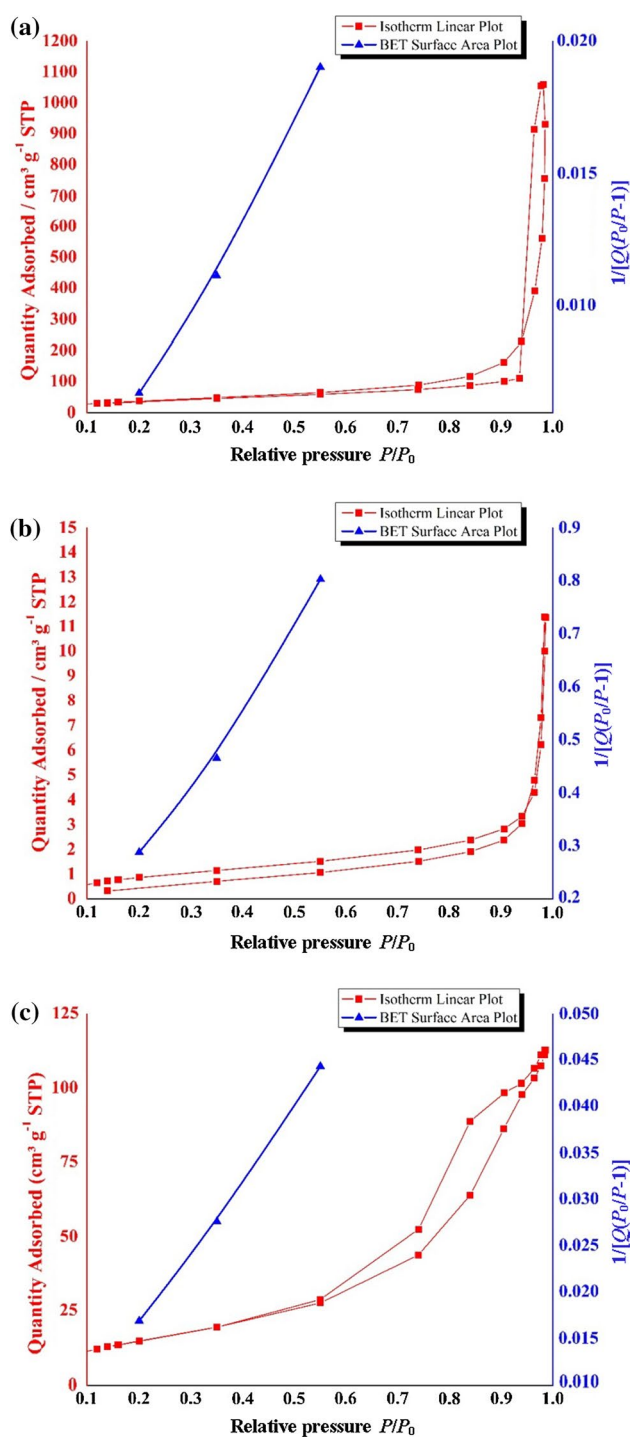
Fig. 5 BET isotherms of M_1 (**a**), M_2 (**b**), and M_3 (**c**)

Table 4 Adsorption–desorption characteristics of M_1–M_3 materials

Materials	BET surface area/m² g⁻¹	BJH pore volume/cm³ g⁻¹	BJH pore width/Å
M_1	125.590	1.588485	531.375
M_2	2.989	0.015653	484.197
M_3	54.815	0.136632	152.692
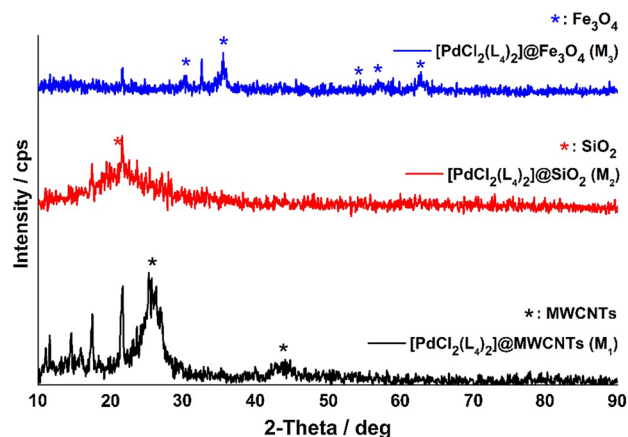
Fig. 6 XRD patterns of M_1 (**a**), M_2 (**b**), and M_3 (**c**)

material (MWCNT, SiO₂, Fe₃O₄). The structure confirms the effectiveness of the simple wet impregnation method for the synthesis MWCNT-, SiO₂-, and Fe₃O₄-supported **C4** materials M_1–M_3.

Catalytic studies

We investigated the catalytic activity of C_1–C_6 complexes using the hydrogenation of 2-nitroaniline (2-NA) to *o*-phenylenediamine in the presence of BH_4^- ion in the water at ambient temperature as a precursor reaction. The functional groups of the synthesized complexes are designed to compare steric, electron-donating and electron-withdrawing groups.

The reaction was easily followed spectrophotometrically due to the reactant (2-NA) and product having different absorption bands such as $\lambda_{max} = 410$ nm [63, 64] (–NO₂ group of 2-NA). Initially, the 2-NA (2.5×10^{-4} mol dm⁻³) mixture has a yellow color which is the color of the adsorption band belonging to the nitro group, this color gradually vanished because of the formation of the *o*-phenylenediamine product. Briefly, the absorption peak at 410 nm gradually decreased in intensity during this reaction. The percent conversions were monitored at different times between 30 and 90 s. It is well known that when the times were increased from minimum time to maximum time. The catalytic efficiencies of C_1–C_6 found as 93.2%, 94.4%, 93.8%, 94.9%,

SiO₂, and Fe₃O₄ materials produced characteristic peaks similar to those of MWCNT [JCDPS card no: 75–1621, 26.29° (002), 43.12° (200), SiO₂ and Fe₃O₄ [JCDPS card no: 19-0629, 30.1° (220), 35.5° (311), 43.1° (400), 57.0° (511), 62.9° (440)] in Fig. 6. Likewise, all the XRD data have new peaks, in addition to the data for pure supporting

Fig. 7 Time-dependent UV–Vis absorption spectra of the 2-nitroaniline reduced by NaBH$_4$ catalyzed by the **C$_1$**–**C$_6$** complexes
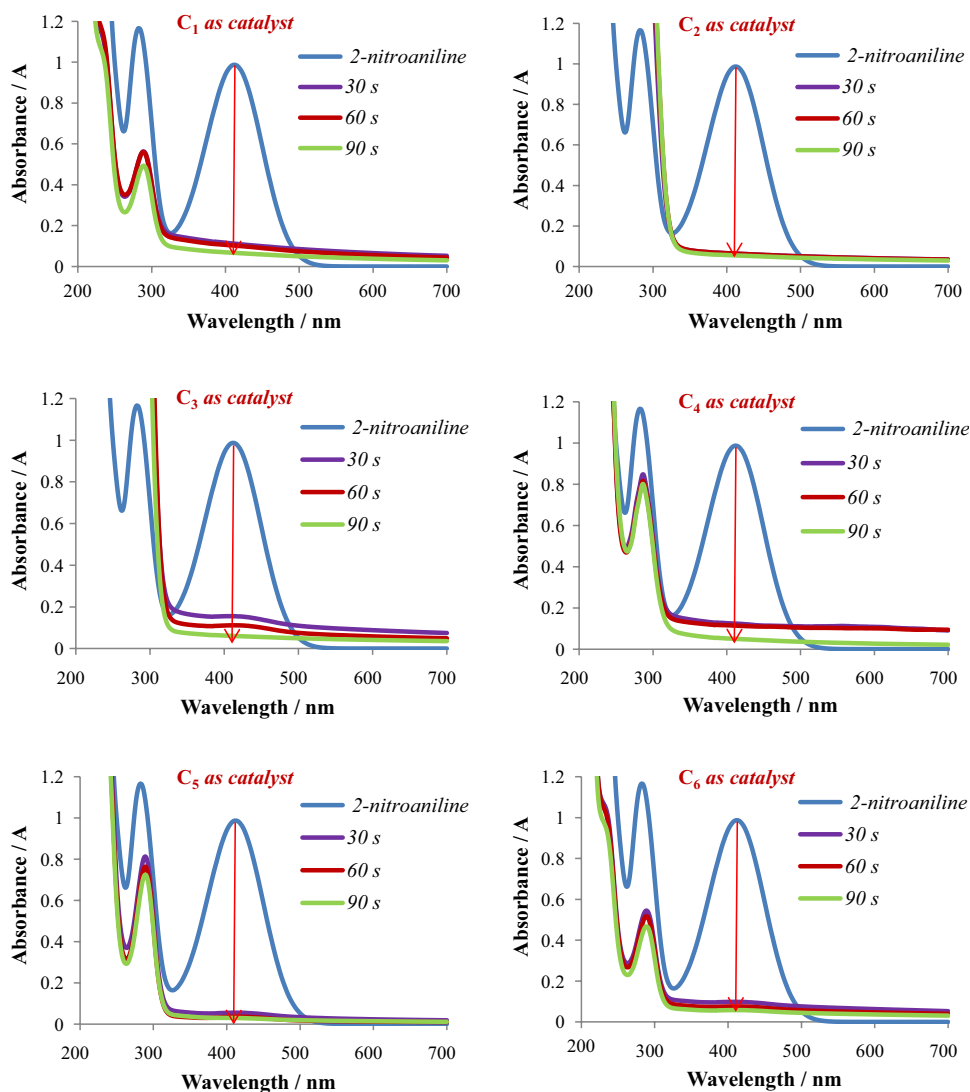

97.0%, and 94.1% at the end of 90 s, respectively (Fig. 7). It is seen that all catalytic reactions were almost complete in 90 s, and so the synthesized Pd(II) complexes **C$_1$**–**C$_6$** were showed excellent catalytic activity under these conditions. A difference in the functional groups could not be determined in all the catalytic activity results obtained. However, the positive contribution of the -F group, an electron-withdrawing group, was detected. Also, the **C$_4$** complex, which shows an average activity in complex selection, was chosen as the representative of the synthesis group. In recent years, the catalytic activity of hybrid materials has been remarkable in the literature [65–70]. In light of this information, we envisaged that the catalytic activity of the tested palladium complexes **C$_1$**–**C$_6$** can be combined with a different type of solid support material such as MWCNTs, SiO$_2$, and Fe$_3$O$_4$ and the performance of these new hybrid materials will be high for the reduction of nitroarenes. Thus, we selected one of the effective palladium complexes (bis[*N*-

(2-aminophenyl)-2,4,6-trimethylbenzenesulfonamide]-dichloro-palladium(II), **C$_4$**) as randomly (not having the best activity) for the impregnation method into MWCNTs, SiO$_2$, and Fe$_3$O$_4$ materials. Herein, the solid support materials selected were selected from different types and their potentials were compared, and the **C$_4$** was chosen for the preparation of solid-supported catalysts, because the supporting material generally increases the efficiency of catalysts synergistically and we also want to clearly demonstrate this effect in this paper. The materials were chosen SiO$_2$ as the most common material, Fe$_3$O$_4$ as a metal oxide with magnetic properties, and MWCNTs as a carbon based and commonly used material.

To demonstrate the success of this methodology, the catalytic performances of bare solid support materials (MWCNTs, SiO$_2$, and Fe$_3$O$_4$) were tested as catalysts under the same conditions which were followed by UV–Vis spectrophotometer in the presence of NaBH$_4$ in water with 2-NA

Fig. 8 Time-dependent UV–Vis absorption spectra of the 2-nitroaniline reduced by NaBH$_4$ catalyzed by the MWCNT, SiO$_2$, and Fe$_3$O$_4$ supported materials
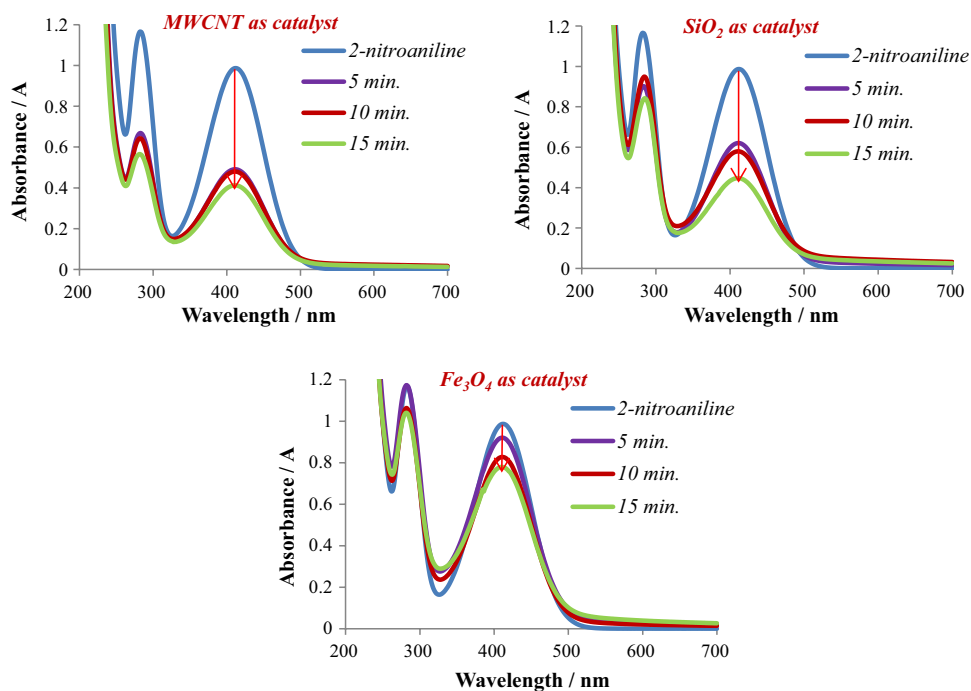
(Fig. 8). When the time-dependent spectrophotometer measurement results are evaluated, the catalytic performances were 50.2% (5 min), 51.4% (10 min), and 58.2% (15 min) for MWCNTs, 37.1% (5 min), 41.3% (10 min), and 54.7% (15 min) for SiO$_2$, 6.7% (5 min), 16.1% (10 min), and 20.9% (15 min) for Fe$_3$O$_4$. In light of these results, it can be said clearly that the catalytic conversion of bare Fe$_3$O$_4$ material is

lower than other selected solid support materials. However, as known, catalysts bearing Fe$_3$O$_4$ can be recovered easily due to the magnetic properties of Fe$_3$O$_4$ (via a simple magnet). Therefore, efforts to improve the catalytic performance power belonging to Fe$_3$O$_4$ material can be quite valuable.

Based on the above results, we tested the catalytic activity of **M$_1$**–**M$_3$** nanomaterials for the catalytic hydrogenation

Fig. 9 Time-dependent UV–Vis absorption spectra of the 2-nitroaniline reduced by NaBH$_4$ catalyzed by the **M$_1$**–**M$_3$**
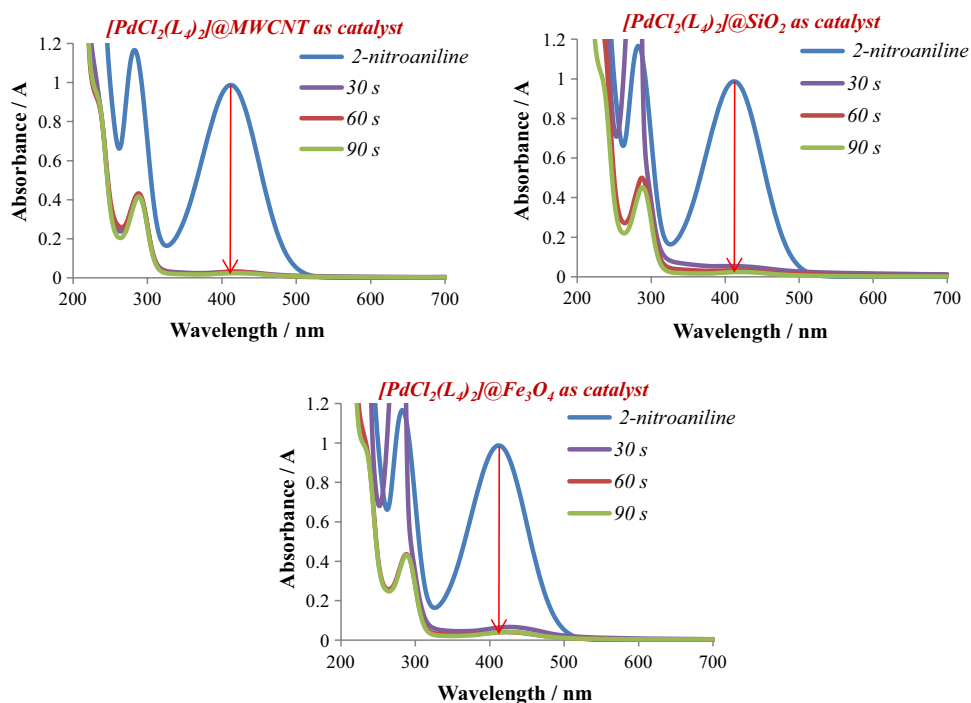
of 2-nitroaniline (2-NA). As shown in Fig. 9, the specific absorption band belonging to 2-nitroaniline is observed 410 nm and when M_1–M_3 nanomaterials were added to the reaction media, the corresponding peak intensity showed a quick decline. The catalytic performances of M_1–M_3 nanomaterials for the hydrogenation of 2-NA were 96.8% (30 s), 96.9% (60 s), 97.7% (90 s); 94.5% (30 s), 96.7% (60 s), 97.6% (90 s); and 93.7% (30 s), 96.0% (60 s), 96.1% (90 s), respectively. A significant improvement in the catalytic performance of the nanomaterials M_1–M_3 was observed compared to bare materials. Interestingly, the best-enhanced catalyst was recorded as M_3 compared to bare Fe_3O_4. These results are compatible with the literature [71]. However, the success of hybrid materials formed by molecular metal complexes is limited [63]. When the catalytic performances of C_4, the bare solid support materials and the hybrid nanomaterials M_1–M_3 are examined in detail, it is evident that the hybrid nanomaterials have higher catalytic conversions than both the palladium(II) complex C_4 and the solid support materials (MWCNTs, SiO_2, Fe_3O_4). This situation may be related to the synergistic effect.

We also studied the hydrogenation of 4-nitroaniline (4-NA) using M_1–M_3 under the same conditions. The characteristic absorption band of the pure 4-nitroaniline arises at 380 nm from the $-NO_2$ group. After the addition of catalysts M_1–M_3, the characteristic band of 4-NA at 380 nm gradually decreased in intensity and the color of the solution gradually vanished as the reaction proceeded. The catalytic activities were found to be 96.7% (30 s),

97.8% (60 s), 98.1% (90 s) for M_1, 96.0% (30 s), 97.1% (60 s), 97.5% (90 s) for M_2, and 96.0% (30 s), 96.8% (60 s), 97.4% (90 s) for M_3 (Fig. 10).

Moreover, M_1–M_3 nanomaterials were used as catalysts for the hydrogenation of nitrobenzene under the optimized conditions. The band disappeared after hydrogenation at 265 nm from the $-NO_2$ group. The performance of catalysts (M_1–M_3) were 89.7% (30 s), 90.3% (60 s), 93.3% (90 s) for M_1, 89.2% (30 s), 90.4% (60 s), 90.6% (90 s) for M_2, and 90.3% (30 s), 90.5% (60 s), 91.3% (90 s) for M_3 (Fig. 11).

Furthermore, the magnetic catalyst M_3 could be recovered from the reaction mixture by filtration with the help of a magnet and used again in the next cycle. According to Fig. 12, the recovered M_3 magnetic catalyst exhibited good catalytic efficiency for at least five cycles in the hydrogenation of 2-NA with the conversion of 96.1–83.5% during the 90 s.

Herein, the kinetic equation for the reduction of nitrobenzenes to anilines can be represented as $\ln(C_t/C_0) = -kt$, where t is time for the reaction and, k is the apparent first-order rate constant (s^{-1}) in Table 5. Also, the $k' = k/M$ parameter (M: the amount of the catalyst) is introduced for quantitative comparison and the parameter is defined as the ratio of the rate constant k to the weight of the catalyst added [72]. In Table 5, the catalytic activity rate constant parameters were compared for the palladium(II) complexes C_1–C_6 and the nanomaterials M_1–M_3 and summarized. The table showed that the parameters k and k' for the nanomaterials M_1–M_3 are


Fig. 10 Time-dependent UV–Vis absorption spectra of the 4-nitroaniline reduced by $NaBH_4$ catalyzed by the M_1–M_3
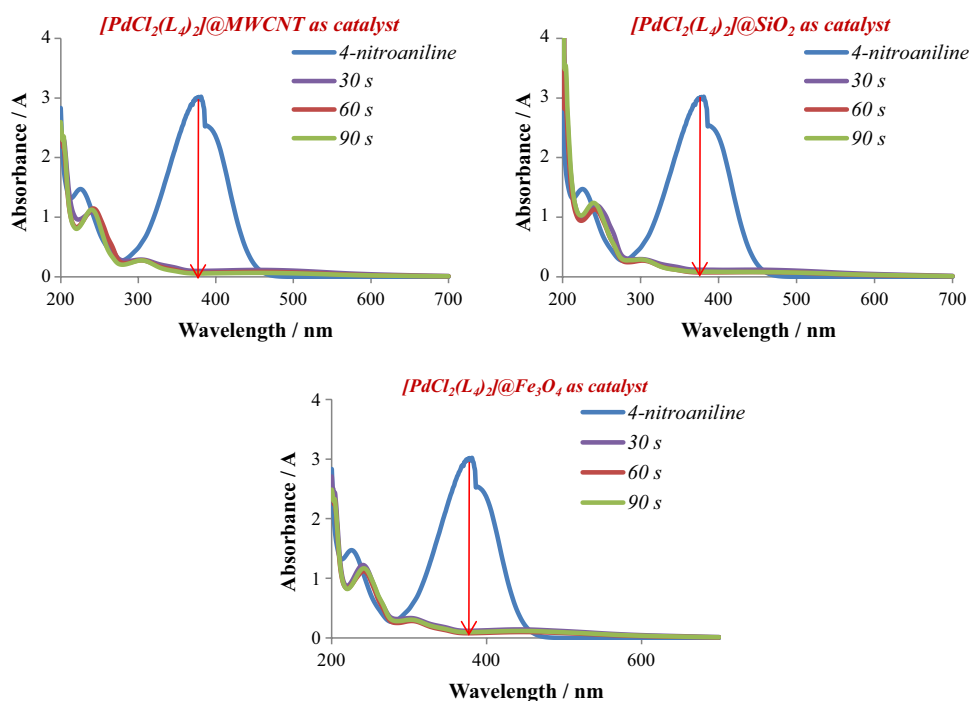
Fig. 11 Time-dependent UV–Vis absorption spectra of the nitrobenzene reduced by NaBH$_4$ catalyzed by the **M$_1$–M$_3$**
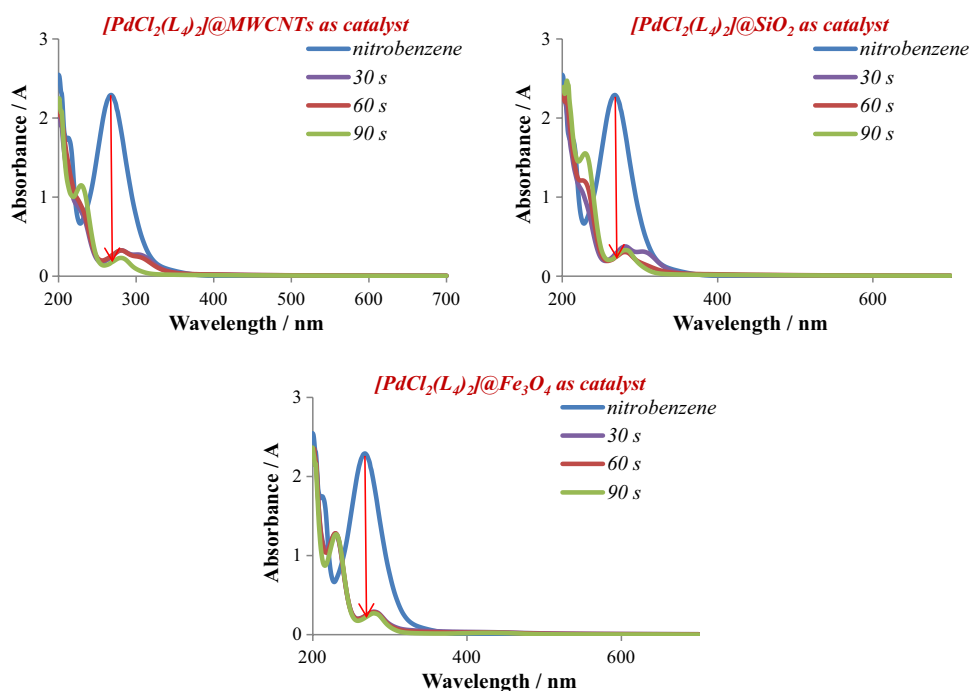
Fig. 12 Reusability of **M$_3$** magnetic catalyst for the hydrogenation of 2-NA with NaBH$_4$ (at 90 s intervals). % Conversion $= [(A_o - A_t)/A_o] \times 100$, A_o is the absorbance at time $t = 0$
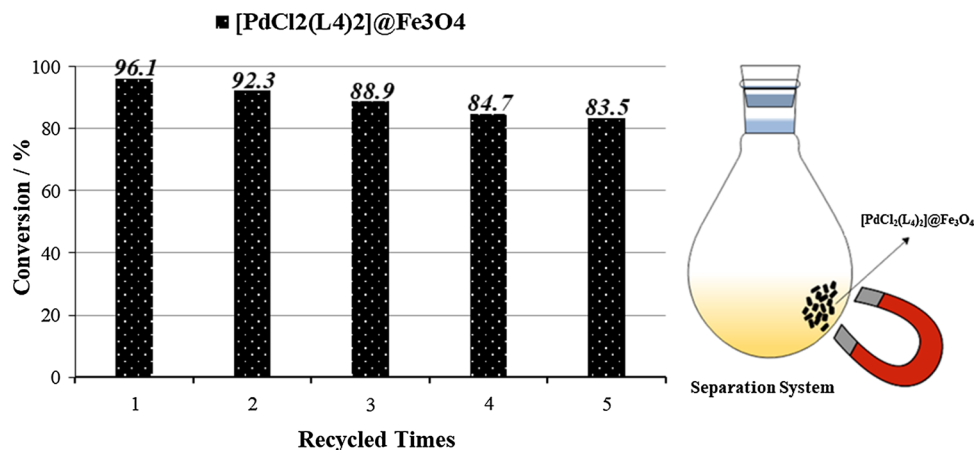
higher than the corresponding palladium(II) complexes and this also supports the synergistic effect during the reduction reaction of nitrobenzenes.

As a general concept, the catalytic activity in any reaction depends on both the composition-type of catalyst and substrate which is detailed in the literature. A catalyzed process is controlled by different parameters in the catalytic system such as particle size (micro or nano), recovery, active surface area, reusability, surface morphology, active functional groups, the redox and electron charge potential of metal center [73]. Materials containing metal ion can appear to be especially efficient catalysts for the reduction of nitroarene or nitrobenzene compounds to aminobenzenes [15, 17, 74, 75]. The hydrogenation or reduction of nitrobenzenes has different mechanisms or pathways and potential

intermediates [25, 76]. The catalyzed process/cycle began immediately by adding **M$_1$–M$_3$** nanomaterials to the reaction mixture. The nitrobenzenes and ions belonging to NaBH$_4$ are diffused from the reaction solution to the active surface of **M$_1$–M$_3$** nanomaterials and especially, around the Pd(II) ion.

Hence, the metal center (palladium(II)) and other regions (ligand and solid material) act as a tool for electron transfer from hydride ions to the nitro group which achieves the formation of the amino group. With this route, the H$^+$ ions are exposed in the reaction medium for the reduction of nitrobenzenes to aminobenzenes and as the cycle rate increases, the reaction rate constant also rises. With this operation, it is clear that the catalytic cycle was rapid with the **M$_1$–M$_3$** nanomaterials compared to bare MWCNTs,

Table 5 Catalytic activity rate constant of catalysts

Catalysts	Substrate	$k/s^{-1 a}$			$k/M/s^{-1}\, g^{-1\, b}$		
		30 s (10^{-2})	60 s (10^{-2})	90 s (10^{-2})	30 s (10^{+1})	60 s (10^{+1})	90 s (10^{+1})
C_1	2-NA	7.24	3.76	2.98	3.62	1.88	1.49
C_2	2-NA	9.10	4.56	3.20	4.55	2.28	1.60
C_3	2-NA	6.16	3.63	3.10	3.08	1.82	1.55
C_4	2-NA	6.91	3.59	3.31	3.46	1.80	1.66
C_5	2-NA	9.63	5.55	3.91	4.82	2.78	1.96
C_6	2-NA	7.69	4.27	3.15	3.85	2.14	1.58
M_1	2-NA	11.60	5.79	4.17	5.80	2.90	2.09
M_2	2-NA	9.68	5.69	4.15	4.84	2.85	2.08
M_3	2-NA	9.19	5.37	3.59	4.60	2.69	1.80
M_1	4-NA	11.40	6.36	4.40	5.70	3.18	2.20
M_2	4-NA	10.80	5.94	4.11	5.40	2.97	2.06
M_3	4-NA	10.70	5.72	4.04	5.35	2.86	2.02
M_1	Nitrobenzene	7.56	3.89	3.00	3.78	1.95	1.50
M_2	Nitrobenzene	7.42	3.91	2.63	3.71	1.96	1.32
M_3	Nitrobenzene	7.77	3.91	2.72	3.89	1.96	1.36

[a]The reaction rate constant

[b]The reaction rate constant per total weight of tested catalyst (2 mg)

SiO_2, Fe_3O_4 materials. There was also a difference in catalytic activity according to the type of substrate. In this reaction medium and conditions, we would recommend that these types of hybrid materials (M_1–M_3) are preferable for the hydrogenation of nitro groups (nitrobenzenes, etc.)

Conclusion

Herein, the fabrication of a series of simple N-coordinate palladium(II) complexes C_1–C_6 and $[PdCl_2(L_4)_2]$@MWC-NTs (M_1), $[PdCl_2(L_4)_2]$@SiO_2 (M_2), and $[PdCl_2(L_4)_2]$@Fe_3O_4 (M_3) nanomaterials and their use as catalysts for the hydrogenation of nitrobenzenes to aminobenzenes was defined. Using a basic impregnation methodology, palladium(II) complexes were immobilized on the surface of MWCNTs, SiO_2, and Fe_3O_4 and detailed structural analysis of the complex and materials was carried out using NMR, UV–Vis, FT-IR, single-crystal X-ray diffraction for C_1, BET, TEM, and XRD methods. The materials M_1–M_3 are highly efficient at room temperature for catalysis of the reduction of nitroanilines (> 95% conversion in < 1 min) with $NaBH_4$ as the hydrogen source in water. Moreover, the M_3 catalyst is highly durable under the optimized conditions for at least five cycles without a significant loss of activity. The catalytic studies carried out with this method have the advantages of high yields, simple synthesis methodology, and easy workup. This type of catalyst is simple and stable, and it can be recovered by an external magnet.

Experimental

All chemicals (reagents and solvents) were purchased from chemical companies (Sigma-Aldrich, Merck, and Alfa Aesar) and used as received unless otherwise stated. Ligands L_1–L_3 [32] and L_4 [77] were synthesized according to the literature.

The 400 MHz ^{1}H NMR and 100.56 MHz ^{13}C NMR spectra were recorded at ambient temperature on a Bruker 400 NMR spectrometer. A Perkin-Elmer Spectrum 400 FT-IR system with universal ATR sampling accessory was used to obtain the FT-IR spectra. For melting point determination, an Electrothermal 9100 instrument was used with open capillary tubes. X-ray diffraction (Bruker AXS D8 Advance Model) was used to confirm for immobilization methodology. The SEM–EDX analysis employed a Leo 440 Computer Controlled Digital for surface morphological characterization. The UV–Vis spectrophotometer (Perkin-Elmer Lambda 25 UV/Vis spectrophotometers) measurements were used for monitoring the reduction of nitrophenols and dyes.

General procedure for the synthesis of ligands L_5 and L_6

A solution of 1,2-diaminobenzene (1 mmol) and triethylamine (2 mmol) in 10 cm³ tetrahydrofuran (THF) was stirred at ambient temperature for 30 min. To this, a solution of aromatic sulfonyl chlorides (1 mmol) in 5 cm³ THF was added slowly under ambient temperature overnight. The resulting solution was filtered, and the volatiles were

removed in vacuo. The material was taken up in 20 cm^3 dichloromethane (DCM), washed with water (3×5 cm^3) and brine (2×5 cm^3), dried over MgSO$_4$, and concentrated under reduced pressure. The product was recrystallized from DCM/diethyl ether (Scheme 1).

N-(2-Aminophenyl)-4-fluorobenzenesulfonamide (L₅, C₁₄H₁₅FN₂S)

Color: orange; yield: 75%; m.p.: 96–97 °C; ^{1}H NMR (400 MHz, CDCl$_3$): $\delta = 4.00$ (br., 2 H, –NH_2), 6.52 (d, 1H, $J = 8$ Hz, –H_1), 6.51 (t, 2H, $J = 8$ Hz, –H_3), 6.73 (d, 1H, $J = 8$ Hz, –H_4), 7.05 (t, 1H, $J = 8$ Hz, –H_2), 7.12 (t, 2H, $J = 8$ Hz, –H_b), 7.77 (d, 2H, $J = 8$ Hz, –H_a) ppm; ^{13}C NMR (100 MHz, CDCl$_3$): $\delta = 116.1$, 117.1, 118.6, 120.7, 128.5, 129.1, 130.3, 134.9, 144.5, 165.3 (d, $J = 260$ Hz) (–C–F) ppm; FT-IR (ATR): $\bar{v} = 3445$, 3338, 3275, 3103, 3071, 3038, 2988, 1621, 1590, 1491, 1463, 1406, 1383, 1330, 1312, 1292, 1261, 1228, 1211, 1164, 1151, 1124, 1088, 1030, 1013, 930, 899, 834, 817, 787, 745, 726, 708, 685, 670 cm^{-1}.

N-(2-Aminophenyl)-4-chlorobenzenesulfonamide (L₆, C₁₄H₁₅ClN₂S)

Color: brown; yield: 77%; m.p.: 106–107 °C; ^{1}H NMR (400 MHz, CDCl$_3$): $\delta = 3.90$ (br., 2 H, –NH_2), 6.50 (d, 1H, $J = 8$ Hz, –H_1), 6.56 (t, 2H, $J = 8$ Hz, –H_3), 6.76 (d, 1H, $J = 8$ Hz, –H_4), 7.07 (t, 1H, $J = 8$ Hz, –H_2), 7.44 (d, 2H, $J = 8$ Hz, –H_b), 7.70 (d, 2H, $J = 8$ Hz, –H_a) ppm; ^{13}C NMR (100 MHz, CDCl$_3$): $\delta = 117.2$, 118.7, 120.6, 128.5, 129.0, 129.2, 129.3, 137.3, 139.6, 144.4 ppm; FT-IR (ATR): $\bar{v} = 3477$, 3379, 3255, 3094, 3074, 2998, 2954, 2904, 1616, 1587, 1574, 1498, 1476, 1464, 1387, 1335, 1308, 1280, 1253, 1214, 1159, 1124, 1084, 1028, 1014, 1007, 973, 941, 930, 902, 840, 814, 755, 744, 726, 703, 667, 649, 621, 567, 555, 534, 486, 469 cm^{-1}.

General procedure for the synthesis of Pd(II) complexes C₁–C₆

A solution of PdCl$_2$ (0.2 mmol) in 5 cm^3 methanol was slowly transferred to a solution of *N*-(2-aminophenyl)benzenesulfonamides (0.4 mmol) in 5 cm^3 methanol. The mixture was slowly warmed to 50 °C for 30 min, cooled to ambient temperature, and stirred overnight before the removal of the volatiles in vacuo. The crude product was washed with diethyl ether (3×10 cm^3) and dried under reduced pressure to give **C₁–C₆** (Scheme 1).

Bis[N-(2-aminophenyl)benzenesulfonamide]-dichloropalladium(II) (C₁, C₂₈H₃₂Cl₂N₄PdS₂)

Color: light yellow; yield: 79%; m.p.: 310–311 °C; ^{1}H NMR (400 MHz, DMSO-d_6): $\delta = 6.58$ (s, 4H, –NH_2), 6.72 (t, 2H, $J = 8$ Hz, –H_3), 6.94 (t, 2H, $J = 8$ Hz, –H_2), 7.07 (d, 2H, $J = 8$ Hz, –H_1), 7.46 (d, 2H, $J = 8$ Hz, –H_4), 7.51 (d, 4H, $J = 8$ Hz, –H_b), 7.99 (d, 4H, $J = 8$ Hz, –H_a) ppm; ^{13}C NMR (100 MHz, DMSO-d_6): $\delta = 117.1$, 121.1, 126.8, 128.8, 129.9, 131.5, 133.8, 138.1, 143.0, 147.2 ppm; FT-IR (ATR): $\bar{v} = 3252$ (–NH$_2$), 3148 (–NH$_2$), 3098 (-NH), 3030, 1608, 1570, 1488, 1454, 1445, 1303, 1286, 1264, 1243, 1208, 1174, 1161, 1141, 1117, 1107, 1081, 1039, 1022, 999, 978, 958, 862, 848, 818, 773, 749, 719, 703, 686 cm^{-1}; UV–Vis (DMSO, $c = 1 \times 10^{-4}$ mol dm^{-3}): λ_{max} (ε) = 280 (9831), 327 (5611) nm (mol^{-1} dm^3 cm^{-1}).

CCDC 1,483,076 contains supplementary crystallographic data for the compound **C₁** reported in this article.

Scheme 1
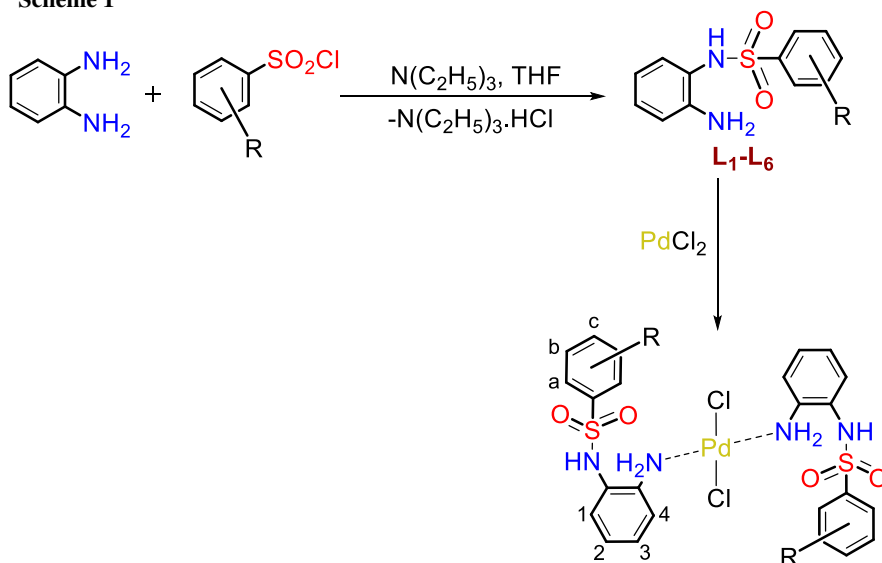
R = 4-H (**C₁**), 4-OCH₃ (**C₂**), 4-NO₂ (**C₃**), 2,4,6-trimethyl (**C₄**), 4-F (**C₅**), 4-Cl (**C₆**)

These data can be obtained free of charge via https://www.ccdc.cam.ac.uk/conts/retrieving.html, or from the Cambridge Crystallographic Data Centre, 12 Union Road, Cambridge CB2 1EZ, UK; fax: (+ 44) 1223-336-033; or e-mail: deposit@ccdc.cam.ac.uk.

Bis[*N*-(2-aminophenyl)-4-methoxybenzenesulfonamide]-dichloro-palladium(II) (C₂, $C_{30}H_{36}Cl_2N_4O_2PdS_2$) Color: yellow; yield: 71%; m.p.: 308–309 °C; ^{1}H NMR (400 MHz, DMSO-d_6): $\delta = 3.43$ (br., 2H, –NH), 3.82 (s, 6H, –OCH_3), 6.50 (t, 2H, $J = 8$ Hz, –H_3), 6.58 (s, 4H, -NH_2), 6.64 (d, 2H, $J = 8$ Hz, –H_1), 6.70 (d, 2H, $J = 8$ Hz, –H_4), 6.92 (t, 2H, $J = 8$ Hz, –H_2), 7.07 (d, 4H, $J = 8$ Hz, –H_b), 7.60 (d, 4H, $J = 8$ Hz, –H_a) ppm; ^{13}C NMR (100 MHz, DMSO-d_6): $\delta = 55.6$ (–OCH_3), 113.8, 114.1, 126.9, 127.4, 128.7, 129.0, 131.5, 135.2, 141.9, 162.3 ppm; FT-IR (ATR): $\bar{v} = 3279$ (–NH$_2$), 3216 (–NH$_2$), 3165 (–NH$_2$), 3131 (–NH), 3072, 2996, 2974, 1593, 1574, 1496, 1463, 1445, 1406, 1332, 1311, 1282, 1261, 1248, 1182, 1149, 1129, 1088, 1030, 1009, 982, 945, 906, 835, 802, 794, 761, 750, 724, 669 cm^{-1}; UV–Vis (DMSO, $c = 1 \times 10^{-4}$ mol dm^{-3}): λ_{max} (ε) = 300 (12,902), 326 (6934) nm (mol^{-1} dm^3 cm^{-1}).

Bis[*N*-(2-aminophenyl)-4-nitrobenzenesulfonamide]-dichloro-palladium(II) (C₃, $C_{28}H_{30}Cl_2N_6O_4PdS_2$) Color: dark yellow; yield: 79%; m.p.: 311–312 °C; ^{1}H NMR (400 MHz, DMSO-d_6): $\delta = 6.99$ (s, 4H, –NH_2), 6.48 (t, 2H, $J = 8$ Hz, –H_3), 6.68 (d, 2H, $J = 8$ Hz, –H_1), 6.99 (d, 2H, $J = 8$ Hz, –H_4), 7.16 (t, 2H, $J = 8$ Hz, –H_2), 7.91 (d, 4H, $J = 8$ Hz, –H_b), 8.37 (d, 4H, $J = 8$ Hz, –H_a) ppm; ^{13}C NMR (100 MHz, DMSO-d_6): $\delta = 124.2$, 124.4, 126.4, 127.1, 127.5, 128.0, 128.5, 141.3, 145.7, 149.7 ppm; FT-IR (ATR): $\bar{v} = 3300$ (–NH$_2$), 3246 (–NH$_2$), 3216 (–NH$_2$), 3147 (-NH), 3103, 3072, 1607, 1578, 1527, 1498, 1478, 1466, 1414, 1401, 1367, 1351, 1340, 1318, 1303, 1292, 1280, 1249, 1238, 1167, 1117, 1088, 1044, 1031, 1014, 949, 938, 914, 853, 832, 796, 764, 748, 738, 716, 699, 682, 663 cm^{-1}; UV–Vis (DMSO, $c = 1 \times 10^{-4}$ mol dm^{-3}): λ_{max} (ε) = 295 (1668), 336 (6314) nm (mol^{-1} dm^3 cm^{-1}).

Bis[*N*-(2-aminophenyl)-2,4,6-trimethylbenzenesulfonamide]-dichloro-palladium(II) (C₄, $C_{34}H_{44}Cl_2N_4PdS_2$) Color: yellow; yield: 75%; m.p.: 256–257 °C; ^{1}H NMR (400 MHz, DMSO-d_6): $\delta = 2.24$ (s, 6H, -p-CH_3), 2.38 (s, 12H, o-CH_3), 6.45 (d, 2H, $J = 8$ Hz, –H_1), 6.60 (t, 2H, $J = 8$ Hz, –H_3), 6.75 (d, 2H, $J = 8$ Hz, –H_4), 6.81 (t, 2H, $J = 8$ Hz, –H_2), 6.98 (s, 4H, –H_b) ppm; ^{13}C NMR (100 MHz, DMSO-d_6): $\delta = 20.5$, 22.6, 116.7, 119.8, 127.7, 131.6, 134.2, 137.1, 138.8, 140.4, 141.7, 147.3 ppm; FT-IR (ATR): $\bar{v} = 3269$ (–NH$_2$), 3185 (–NH$_2$), 3153 (–NH), 3070, 2987, 2940, 1599, 1494, 1465, 1453, 1408, 1393, 1382, 1332, 1299, 1274, 1246, 1191, 1161, 1138, 1117, 1105,

1052, 1043, 1038, 1023, 958, 894, 864, 853, 792, 753, 716, 672, 660 cm^{-1}; UV–Vis (DMSO, $c = 1 \times 10^{-4}$ mol dm^{-3}): λ_{max} (ε) = 289 (13,725), 335 (6553) nm (mol^{-1} dm^3 cm^{-1}).

Bis[*N*-(2-aminophenyl)-4-fluorobenzenesulfonamide]-dichloro-palladium(II) (C₅, $C_{28}H_{30}Cl_2F_2N_4PdS_2$) Color: dark yellow; yield: 73%; m.p.: 260–261 °C; ^{1}H NMR (400 MHz, DMSO-d_6): $\delta = 6.56$ (s, 4H, –NH_2), 6.75 (t, 2H, $J = 8$ Hz, –H_3), 6.96 (t, 2H, $J = 8$ Hz, –H_2), 7.07 (d, 2H, $J = 8$ Hz, –H_1), 7.35 (4H, –H_b), 7.50 (d, 2H, $J = 8$ Hz, –H_4), 8.02 (4H, –H_a) ppm; ^{13}C NMR (100 MHz, DMSO-d_6): $\delta = 115.7$, 120.9, 125.9, 126.6, 129.6, 135.7, 139.5, 141.3, 147.0, 163.6 (d, $J = 240$ Hz) (–C–F) ppm; FT-IR (ATR): $\bar{v} = 3221$ (–NH$_2$), 3153 (–NH$_2$), 3109 (–NH), 3081, 3013, 2829, 2781, 1615, 1590, 1574, 1539, 1492, 1455, 1403, 1306, 1296, 1289, 1272, 1252, 1235, 1216, 1192, 1166, 1144, 1127, 1112, 1098, 1081, 1042, 1029, 1012, 981, 960, 858, 843, 830, 813, 763, 743, 709, 701, 679, 664 cm^{-1}; UV–Vis (DMSO, $c = 1 \times 10^{-4}$ mol dm^{-3}): λ_{max} (ε) = 301 (13,291), 335 (7698) nm (mol^{-1} dm^3 cm^{-1}).

Bis[*N*-(2-aminophenyl)-4-chlorobenzenesulfonamide]-dichloro-palladium(II) (C₆, $C_{28}H_{30}Cl_4N_4PdS_2$) Color: light yellow; yield: 71%; m.p.: 331–332 °C; ^{1}H NMR (400 MHz, DMSO-d_6): $\delta = 6.55$ (s, 4H, –NH_2), 6.75 (t, 2H, $J = 8$ Hz, –H_3), 6.97 (t, 2H, $J = 8$ Hz, –H_2), 7.06 (d, 2H, $J = 8$ Hz, –H_1), 7.51 (d, 2H, $J = 8$ Hz, –H_4), 7.58 (d, 4H, $J = 8$ Hz, –H_b), 7.95 (d, 4H, $J = 8$ Hz, –H_a) ppm; ^{13}C NMR (100 MHz, DMSO-d_6): $\delta = 121.0$, 121.4, 125.9, 126.5, 128.6, 128.8, 135.7, 136.1, 142.0, 146.9 ppm; FT-IR (ATR): $\bar{v} = 3247$ (–NH$_2$), 3185 (–NH$_2$), 3152 (–NH), 3102, 2908, 1612, 1574, 1489, 1476, 1456, 1394, 1306, 1293, 1266, 1240, 1208, 1169, 1142, 1115, 1107, 1080, 1037, 1014, 983, 949, 865, 847, 821, 811, 774, 748, 709, 648 cm^{-1}; UV–Vis (DMSO, $c = 1 \times 10^{-4}$ mol dm^{-3}): λ_{max} (ε) = 287 (12,236) nm (mol^{-1} dm^3 cm^{-1}).

General procedure for the preparation of MWCNT, SiO₂, and Fe₃O₄-supported C₄ (M₁–M₃)

C_4@MWCNTs (M_1), C_4@SiO$_2$ (M_2), and C_4@Fe$_3$O$_4$ (M_3) materials were prepared by modifying the published procedure [37, 63, 78]. Raw MWCNTs (698,849 Aldrich) was refluxed with a magnetic stirrer in a mixture of HNO$_3$ (78%) and H$_2$SO$_4$ (98%) (1/3 v/v) at 130 °C. This process ensured the formation of the carboxylic acid (R–COOH) groups on the sidewalls of MWCNTs. The final product MWCNTs–COOH was filtered and washed with pure water (5 cm^3, five times), and dried under reduced pressure at 40 °C [37].

In a 20 cm^3 glass tube, 90 mg of MWCNTs, SiO$_2$, or Fe$_3$O$_4$ (from FeCl$_3$·6H$_2$O and FeSO$_4$·4H$_2$O with stoichiometric ratios in the presence of ammonia in water [71]) was

dispersed in 10 cm^3 of diethyl ether via an ultrasonic device, and then 10 mg of **C$_4$** complex as a model complex (this weight ratio was selected to set the amount of catalyst used in each catalytic experiment) was added to the pot. The final mixture was sonicated for 3 h to form a stable suspension at ambient temperature. Then, the volatiles were evaporated in vacuo and dried under reduced pressure. The prepared materials were structurally analyzed by FT-IR, TEM, BET, and XRD.

Catalytic reduction of nitroarenes

The catalytic activities of **C$_1$–C$_6$** and **M$_1$–M$_3$** were examined for the reduction of nitroarenes (2-nitroaniline, 2-NA, 4-nitroaniline, 4-NA, nitrobenzene, NB) to aminoarenes in the presence of NaBH$_4$ as a hydrogen source in the water at ambient temperature.

In a typical reduction reaction, 2.5 mg of the catalysts were added to nitroarenes (2.5×10^{-4} mol dm^{-3}) and NaBH$_4$ (0.015 M, freshly) in aqueous solution (10 mol dm^{-3}) and stirred at ambient temperature for a period of the desired time. It is important that the reaction started instantly after the addition of the catalyst. At the end of the period followed, the samples are taken from the reaction and filtered through the micro column. The progress of the reaction was monitored using an ultraviolet–visible (UV–Vis) spectrophotometer (Perkin-Elmer Lambda 25). The catalytic activities of all the materials were monitored by comparing the bands which appeared and disappeared after reduction on the UV–Vis spectrum.

References

1. Dell'Anna MM, Intini S, Romanazzi G, Rizzuti A, Leonelli C, Piccinni F, Mastrorilli P (2014) J Mol Catal A Chem 395:307
2. Hu XW, Long Y, Fan MY, Yuan M, Zhao H, Ma JT, Dong ZP (2019) Appl Catal B Environ 244:25
3. Shokouhimehr M, Kim T, Jun SW, Shin K, Jang Y, Kim BH, Kim J, Hyeon T (2014) Appl Catal A Gen 476:133
4. Das P, Ghosh S, Baskey M (2019) J Mater Sci Mater Electron 30:19731
5. Qu YM, Chen T (2020) Chem Eng J 382:122911
6. Liu Q, Tadrent S, Proust C, Gomez F, Khelfa A, Luart D, Len C (2020) Chem Eng Sci 211:115275
7. Du JT, Shi J, Sun Q, Wang D, Wu H, Wang JX, Chen JF (2020) Chem Eng J 382:122883
8. Marais E, Nyokong T (2008) J Hazard Mater 152:293
9. Modirshahla N, Behnajady MA, Mohammadi-Aghdam S (2008) J Hazard Mater 154:778
10. Canizares P, Saez C, Lobato J, Rodrigo MA (2004) Ind Eng Chem Res 43:1944
11. Chiou JR, Lai BH, Hsu KC, Chen DH (2013) J Hazard Mater 248:394
12. Khan F, Pandey J, Vikram S, Pal D, Cameotra SS (2013) J Hazard Mater 254:72
13. Jayabal S, Ramaraj R (2014) Appl Catal A Gen 470:369
14. Baran T (2019) J Mol Struct 1182:213
15. Liu ZY, Wang XG, Zou XJ, Lu XG (2018) ChemistrySelect 3:5165
16. Jia WG, Ling S, Zhang HN, Sheng EH, Lee R (2018) Organometallics 37:40
17. Cui XL, Zhou X, Dong ZP (2018) Catal Commun 107:57
18. Oh SG, Mishra V, Cho JK, Kim BJ, Kim HS, Suh YW, Lee H, Park HS, Kim YJ (2014) Catal Commun 43:79
19. Schabel T, Belger C, Plietker B (2013) Org Lett 15:2858
20. Fan GY, Huang WJ, Wang CY (2013) Nanoscale 5:6819
21. Nasrollahzadeh M, Sajadi SM, Rostami-Vartooni A, Alizadeh M, Bagherzadeh M (2016) J Colloid Interf Sci 466:360
22. Naseem K, Begum R, Farooqi ZH (2017) Environ Sci Pollut Res 24:6446
23. Dong BQ, Li YH, Ning XM, Wang HJ, Yu H, Peng F (2017) Appl Catal A Gen 545:54
24. Jiang T, Du SC, Jafari T, Zhong W, Sun Y, Song WQ, Luo Z, Hines WA, Suib SL (2015) Appl Catal A Gen 502:105
25. El-Hout SI, El-Sheikh SM, Hassan HMA, Harraz FA, Ibrahim IA, El-Sharkawy EA (2015) Appl Catal A Gen 503:176
26. Dayan S, Altinkaynak C, Kayaci N, Dogan SD, Özdemir N, Ozpozan NK (2020) Appl Organomet Chem 34:e5381
27. Dayan S, Kayaci N, Dayan O, Ozdemir N, Ozpozan NK (2020) Polyhedron 175:114181
28. Dongil AB, Pastor-Perez L, Fierro JLG, Escalona N, Sepulveda-Escribano A (2016) Appl Catal A Gen 513:89
29. Areephong J, Huo B, Mbaezue II, Ylijoki KEO (2016) Tetrahedron Lett 57:3124
30. Khan RI, Pitchumani K (2016) Green Chem 18:5518
31. Ji R, Zhai SR, Zheng W, Xiao ZY, An QD, Zhang F (2016) RSC Adv 6:70424
32. Dayan S, Kalaycioglu NO (2013) Appl Organomet Chem 27:52
33. McCue AJ, Guerrero-Ruiz A, Rodriguez-Ramos I, Anderson JA (2016) J Catal 340:10
34. Dahm G, Bailly C, Karmazin L, Bellemin-Laponnaz S (2015) J Organomet Chem 794:115
35. Marquise N, Chevallier F, Nassar E, Frederich M, Ledoux A, Halauko YS, Ivashkevich OA, Matulis VE, Roisnel T, Dorcet V, Mongin F (2016) Tetrahedron 72:825
36. Rezaei B, Shams-Ghahfarokhi L, Havakeshian E, Ensafi AA (2016) Talanta 158:42
37. Dayan S, Ozdemir N, Ozpozan NK (2019) Appl Organomet Chem 33:e4710
38. Charbonneau M, Addoumieh G, Oguadinma P, Schmitzer AR (2014) Organometallics 33:6544
39. Dang TT, Zhu YH, Ngiam JSY, Ghosh SC, Chen AQ, Seayad AM (2013) ACS Catal 3:1406
40. Kim SW, Kim M, Lee WY, Hyeon T (2002) J Am Chem Soc 124:7642
41. Zeng MF, Wang YD, Liu Q, Yuan X, Feng RK, Yang Z, Qi CZ (2016) Int J Biol Macromol 89:449
42. Choi J, Chan S, Yip G, Joo H, Yang H, Ko FK (2016) Water Res 101:46
43. Pahlevanneshan Z, Moghadam M, Mirkhani V, Tangestaninejad S, Mohammadpoore-Baltork I, Loghmani-Khouzani H (2016) J Organomet Chem 809:31
44. Morisse CGA, McInroy AR, Anderson C, Mitchell CJ, Parker SF, Lennon D (2017) Catal Today 283:110
45. Yadav D, Awasthi SK (2020) New J Chem 44:1320
46. Subodh, Mogha NK, Chaudhary K, Kumar G, Masram DT (2018) ACS Omega 3:16377
47. Subodh, Chaudhary K, Prakash K, Masram DT (2020) Appl Surf Sci 509:144902
48. Dayan S, Kayaci N, Ozpozan NK, Dayan O (2017) Appl Organomet Chem 31:e3699

49. Kayaci N, Dayan S, Ozdemir N, Dayan O, Ozpozan NK (2018) Appl Organomet Chem 32:e4558

50. Gunnaz S, Ozdemir N, Dayan S, Dayan O, Cetinkaya B (2011) Organometallics 30:4165

51. Sheldrick GM (2015) Acta Crystallogr A 71:3

52. Sheldrick GM (2015) Acta Crystallogr C 71:3

53. Farrugia LJ (2012) J Appl Crystallogr 45:849

54. Vicente J, Saura-Llamas I, Garcia-Lopez JA (2010) Organometallics 29:4320

55. Accadbled F, Tinant B, Henon E, Carrez D, Croisy A, Bouquillon S (2010) Dalton Trans 39:8982

56. Grazul M, Sigel R, Maake C, Besic-Gyenge E, Lorenz IP, Mayer P, Czyz M, Budzisz E (2014) Polyhedron 67:136

57. Sabater S, Mata JA, Peris E (2013) Organometallics 32:1112

58. Wu QX, Wu LL, Zhang L, Fu HY, Zheng XL, Chen H, Li RX (2014) Tetrahedron 70:3471

59. Tessier C, Rochon FD (2010) Inorg Chim Acta 363:2652

60. Heinrich F, Kessler MT, Dohmen S, Singh M, Prechtl MHG, Mathur S (2012) Eur J Inorg Chem 36:6027

61. Grirrane A, Garcia H, Corma A, Alvarez E (2012) Chem Eur J 18:14934

62. Bernstein J, Davis RE, Shimoni L, Chang NL (1995) Angew Chem Int Ed 34:1555

63. Dayan S, Arslan F, Ozpozan NK (2015) Appl Catal B Environ 164:305

64. Dayan S, Ozturk S, Kayaci N, Ozpozan NK, Ozturk E (2015) B Mater Sci 38:1651

65. Kilic A, Gezer E, Durap F, Aydemir M, Baysal A (2019) J Organomet Chem 896:129

66. Zheng Y, He F, Wu JM, Ma DL, Fan HL, Zhu SF, Li X, Lu YZ, Liu Q, Hu X (2019) ACS Appl Nano Mater 2:3538

67. Zhang N, Cao LY, Feng LL, Huang JF, Kajiyoshi K, Li CY, Liu QQ, Yang D, He JJ (2019) Nanoscale 11:11542

68. Yao YJ, Yu MJ, Yin HY, Wei FY, Zhang J, Hu HH, Wang SB (2019) Appl Surf Sci 489:44

69. Xu C, Wang J, Gao BR, Dou MM, Chen R (2019) J Mater Sci 54:8892

70. Tamakloe W, Agyeman DA, Park M, Yang J, Kang YM (2019) J Mater Chem A 7:7396

71. Abbas M, Torati SR, Kim C (2015) Nanoscale 7:12192

72. Baghbamidi SE, Hassankhani A, Sanchooli E, Sadeghzadeh SM (2018) Appl Organomet Chem 32:e4251

73. Goyal A, Bansal S, Singhal S (2014) Int J Hydrogen Energy 39:4895

74. Begum R, Naseem K, Ahmed E, Sharif A, Farooqi ZH (2016) Colloid Surf A 511:17

75. Huang HG, Tang MW, Wang XG, Zhang M, Guo SQ, Zou XJ, Lu XG (2018) ACS Appl Mater Inter 10:5413

76. Mahata N, Cunha AF, Orfao JJM, Figueiredo JL (2008) Appl Catal A Gen 351:204

77. Dayan S, Arslan F, Kayaci N, Kalaycioglu NO (2014) Spectrochim Acta A 120:167

78. Dayan S, Kalaycioglu NO, Dayan O, Ozdemir N, Dincer M, Buyukgungor O (2013) Dalton Trans 42:4957